



Glacial CO₂ decrease and deep-water deoxygenation by iron fertilization from glaciogenic dust

Akitomo Yamamoto^{1,2}, Ayako Abe-Ouchi^{1,2}, Rumi Ohgaito¹, Akinori Ito¹, and Akira Oka²

¹Japan Agency for Marine–Earth Science and Technology, Yokohama, Japan

²Atmospheric and Ocean Research Institute, The University of Tokyo, Kashiwa, Japan

Correspondence: Akitomo Yamamoto (akitomo@jamstec.go.jp)

Received: 4 March 2019 – Discussion started: 7 March 2019

Revised: 15 May 2019 – Accepted: 17 May 2019 – Published: 4 June 2019

Abstract. Increased accumulation of respired carbon in the deep ocean associated with enhanced efficiency of the biological carbon pump is thought to be a key mechanism of glacial CO₂ drawdown. Despite greater oxygen solubility due to seawater cooling, recent quantitative and qualitative proxy data show glacial deep-water deoxygenation, reflecting increased respired carbon accumulation. However, the mechanisms of deep-water deoxygenation and contribution from the biological pump to glacial CO₂ drawdown have remained unclear. In this study, we report the significance of iron fertilization from glaciogenic dust in glacial CO₂ decrease and deep-water deoxygenation using our numerical simulation, which successfully reproduces the magnitude and large-scale pattern of the observed oxygen changes from the present to the Last Glacial Maximum. Sensitivity experiments show that physical changes contribute to only one-half of all glacial deep deoxygenation, whereas the other one-half is driven by iron fertilization and an increase in the whole ocean nutrient inventory. We find that iron input from glaciogenic dust with higher iron solubility is the most significant factor in enhancing the biological pump and deep-water deoxygenation. Glacial deep-water deoxygenation expands the hypoxic waters in the deep Pacific and Indian oceans. The simulated global volume of hypoxic waters is nearly double the present value, suggesting that glacial deep water was a more severe environment for benthic animals than that of the modern oceans. Our model underestimates the deoxygenation in the deep Southern Ocean because of enhanced ventilation. The model–proxy comparison of oxygen change suggests that a stratified Southern Ocean is required for reproducing the oxygen decrease in the deep Southern Ocean. Iron fertilization and a global nutrient increase contribute to

a decrease in glacial CO₂ of more than 30 ppm, which is supported by the model–proxy agreement of oxygen change. Our findings confirm the significance of the biological pump in glacial CO₂ drawdown and deoxygenation.

1 Introduction

The oceanic carbon cycle has been proposed as a driver of glacial–interglacial CO₂ change; however, the magnitude of glacial CO₂ reduction of 80–100 ppm has yet to be fully reproduced by numerical model simulations using both an ocean general circulation model (OGCM) and a biogeochemical model (Ciais et al., 2013). The oceanic soft-tissue biological pump, by which the photosynthetic production, sinking, and remineralization of organic matter store dissolved inorganic carbon in the deep ocean, is among the mechanisms controlling glacial–interglacial as well as future atmospheric CO₂ change (Sarmiento and Gruber, 2006; Sigman et al., 2010; Yamamoto et al., 2018). During glacial periods, the efficiency of the biological pump would have been enhanced by biogeochemical processes (e.g., dust-borne iron fertilization, Martin, 1990; and an increase in nutrient inventory associated with a sea-level drop, Broecker, 1982; Wallmann et al., 2016), leading to the transfer of carbon from the atmosphere to the deep ocean. Although changes in marine productivity during glacial periods and its relationship to the dust deposition flux have been widely supported by proxy records (Kohfeld et al., 2005; Jaccard et al., 2013), there are no direct proxy records of the greater accumulation of respired organic carbon. Thus, the contribution of the biological pump to glacial CO₂ reduction is poorly understood.

Because the dissolved oxygen cycle is the mirror image of the biological carbon cycle (oxygen is produced by photosynthesis and is utilized with consistent stoichiometry through the remineralization of sinking organic matter in the ocean interior), oxygen is consumed in the ocean interior when respired organic carbon accumulates in seawater. Thus, reconstructed oxygen change is useful to constrain the biological pump magnitude and respired carbon accumulation. Proxy data show that, despite greater oxygen solubility due to lower sea surface temperatures (SSTs), oxygen concentrations decreased throughout the deep ocean during the Last Glacial Maximum (LGM) (Jaccard and Galbraith, 2012). This indicates greater oxygen consumption and respired carbon accumulation, which could have been caused by several processes including greater organic matter transport into the deep ocean, increasingly restricted air–sea exchange due to sea-ice expansion, and/or more sluggish ocean circulation. However, previous modeling studies have shown conflicting oxygen changes in LGM simulations (Galbraith and Jaccard, 2015; Schmittner and Somes, 2016; Buchanan et al., 2016; Bopp et al., 2017; Somes et al., 2017; Galbraith and de Lavergne, 2019) and the causes of the oxygen decrease in the deep ocean have not yet been fully explored.

Furthermore, because most observations provide only qualitative estimates of oxygen changes, previous model–proxy comparisons have only discussed the glacial oxygen trend (oxygenation in the upper ocean and deoxygenation in the deep ocean). Several recent studies using $\delta^{13}\text{C}$ in benthic foraminiferal or iodine-to-calcium ratios in planktonic foraminifera were able to quantify oxygen concentration changes (Schmiedl and Mackensen, 2006; Hoogakker et al., 2015, 2018; Gottschalk et al., 2016; Lu et al., 2016; Bunzel et al., 2017; Umling and Thunell, 2018). These quantitative proxy data provide firmer constraints on respired carbon accumulation, such that a quantitative model–proxy comparison of oxygen change is very useful for quantifying the contribution of the biological pump to glacial CO₂ drawdown.

In this study, to quantify the impact of changes in the biological pump on glacial carbon and oxygen cycles, we conducted pre-industrial (PI) and LGM simulations using the coupled atmosphere–ocean general circulation model (Oka et al., 2011), aerosol model (Ohgaito et al., 2018), and ocean biogeochemical model (Yamamoto et al., 2015). We focused here on the iron fertilization process in enhancing the biological pump. We attempted to separately quantify iron fertilization effects from desert dust and glaciogenic dust (derived from glacier erosion). Previous studies using mineral aerosol models suggest that glaciogenic dust significantly contributed to an increase in the dust deposition flux at high latitudes during the LGM (e.g., the glaciogenic dust derived from Patagonian glaciers increased dust deposition in the Southern Ocean; SO) and provided a LGM dust deposition flux distribution more consistent with the reported measurements (Mahowald et al., 2006; Ohgaito et al., 2018). Moreover, the iron solubility in glaciogenic dust ($\sim 3\%$) is much

higher than that in desert dust ($\sim 1\%$) (Schroth et al., 2009); however, the higher solubility effect of glaciogenic dust on iron fertilization was not considered in previous modeling studies. Glaciogenic dust is a significant source of bioavailable iron (Shoenfelt et al., 2018) and would therefore have a major impact on biological productivity in high nutrient and low chlorophyll (HNLC) regions where biological productivity is limited by the lack of iron. We also considered the effect of an increase in macronutrient inventory associated with a glacial sea-level drop of $\sim 120\text{ m}$ (Broecker, 1982; Wallmann et al., 2016). A decrease in the area of continental margins reduced the burial of organic matter in margin sediments, leading to increases in the global inventory of phosphate (PO₄) and nitrate (NO₃). Based on a recent simulation, increases in NO₃ and PO₄ inventories by 15% can be assumed (Wallmann et al., 2016).

We performed several sensitivity experiments as listed in Table 1 to explore the contribution of changes in atmospheric dust and nutrient inventory on glacial carbon and oxygen cycles. Moreover, our modeled oxygen changes were compared to recently reported qualitative (Jaccard and Galbraith, 2012) and quantitative reconstructions (Schmiedl and Mackensen, 2006; Hoogakker et al., 2015, 2018; Gottschalk et al., 2016; Lu et al., 2016; Bunzel et al., 2017; Umling and Thunell, 2018) to evaluate the simulated accumulation of respired carbon. Our simulation shows that glaciogenic dust and increased nutrient inventory play a crucial role in glacial CO₂ decrease and deep-water deoxygenation.

2 Model and experiments

The ocean biogeochemical cycle was calculated using the Model for Interdisciplinary Research on Climate (MIROC)-based offline biogeochemical model, based on Yamamoto et al. (2015), with the implementation of an iron cycle. A one-box atmosphere is coupled to an offline biogeochemical model to predict atmospheric CO₂ concentration through gas exchange between the atmosphere and ocean surface. For the tracer calculation, the model uses prescribed monthly output data of horizontal ocean velocities, vertical diffusivity, temperature, salinity, sea surface height, sea surface wind speed, sea-ice fraction, and sea surface solar radiation derived from PI and LGM simulations conducted by Oka et al. (2011) using the MIROC 4 m coupled atmosphere–ocean general circulation model (AOGCM). Both PI and LGM simulations follow the Paleoclimate Modelling Intercomparison Project phase 2 (PMIP2) protocol (Braconnot et al., 2007). MIROC 4 m simulates the weaker and shallower Atlantic Meridional Overturning Circulation (AMOC) during the LGM (see Fig. 1 in Oka et al., 2011), which is consistent with $\delta^{13}\text{C}$ distributions reported from proxy data (Curry and Oppo, 2005). The horizontal and vertical resolutions of the offline biogeochemical model are the same as those in MIROC 4 m.

Table 1. Description of the model experiments.

Experiments	Climate	Dust deposition	Fe solubility in glaciogenic dust	Dust DFe (Gmol year ⁻¹)	Global PO ₄ (mmol m ⁻³)
PI	PI	PI	–	2.7	2.13
LGM_clim	LGM	PI	–	2.7	2.2 (+3 %)
LGM_dust	LGM	LGMctl	–	8.6	2.2 (+3 %)
LGM_glac3%	LGM	LGMglac	3 %	24.5	2.2 (+3 %)
LGM_glac10%	LGM	LGMglac	10 %	61.6	2.2 (+3 %)
LGM_all	LGM	LGMglac	3 %	24.5	2.45 (+15 %)

This biogeochemical model includes two phytoplankton classes (nitrogen fixers and other phytoplankton), zooplankton, particulate detritus, nitrate (NO₃), phosphate (PO₄), dissolved iron (DFe), dissolved oxygen (O₂), dissolved inorganic carbon (DIC), alkalinity (ALK), two carbon isotopes (¹³C and ¹⁴C), and an ideal age tracer. The ideal age is set to zero at the surface and ages at a rate of 1 year year⁻¹ in the ocean interior. Constant stoichiometry relates the C, N, P, and DFe content of the biological variables and their exchanges to inorganic variables (NO₃, PO₄, DFe, O₂, ALK, and DIC). The maximum phytoplankton growth and microbial remineralization rates are assumed to increase with seawater temperature (Eppley, 1972). The iron cycle that is incorporated in the biogeochemical model mainly follows Parekh et al. (2005). In addition to dust deposition, which is assumed as the only DFe source in Parekh et al. (2005), sedimentary and hydrothermal DFe inputs are considered. When the DFe concentration exceeds the total ligand concentration, a formulation for the DFe scavenging rate of Moore and Braucher (2008) is applied. To obtain a realistic distribution of the iron-limited region, total ligand concentration, which controls the amount of the free form of iron, is set to a global constant value of 0.6 μmol m⁻³ instead of the original value of 1 μmol m⁻³ (Fig. 1a).

Dust deposition flux is obtained from the monthly output data of MIROC Earth system model (ESM) in the PI and LGM simulations (Ohgaito et al., 2018). Dust is assumed to contain a constant fraction of iron (3.5 wt %); 1 % of the iron in desert dust is assumed to instantaneously dissolve at the sea surface. The global DFe flux from dust in the PI is 2.7 Gmol year⁻¹ (Table 1). We used two sets of LGM dust deposition flux labeled as LGMctl and LGMglac as calculated in a previous study (Ohgaito et al., 2018). LGMctl is the standard LGM simulation, which has been submitted to Coupled Model Intercomparison Project phase 5/PMIP phase 4 (CMIP5/PMIP4). LGMglac is identical to LGMctl, except that an additional glaciogenic dust flux based on Mahowald et al. (2006) is included. In LGMctl, the dust deposition flux is underestimated in North America, Eurasia, the South Pacific, the SO, and Antarctica compared to the proxy data of ice and sediment cores (Kohfeld et al., 2013; Albani et al., 2014). Because glaciogenic dust increases dust deposition at high latitudes, the underestimation is generally improved in

LGMglac (see Ohgaito et al., 2018, for more details). The global DFe fluxes from dust are 8.6 and 13.9 Gmol year⁻¹ for LGMctl and LGMglac, respectively.

Present observation generally shows a lower Fe solubility at a higher Fe concentration in aerosols and a higher solubility at a lower concentration (Fig. S1 in the Supplement). A wider range of aerosol Fe solubility (from 0.2 % to 48 %) has been derived from observations over the SO, but different types of Fe-containing minerals such as pyrogenic Fe oxides can be considered to achieve high Fe solubilities (Ito et al., 2019). Thus, an assumed constant iron solubility of 2 % in all types of dust could lead to overestimation of a total DFe flux from different types of Fe-containing aerosols during the LGM (Muglia et al., 2017). However, a much higher Fe solubility (1 %–42 % of Fe solubility) as derived from observations for the LGM aerosols in Antarctica has suggested that an assumed constant iron solubility of 1 %–2 % for all types of dust could lead to a DFe flux underestimation during the LGM (Conway et al., 2015). In LGM_glac3%, an iron solubility of 3 % in glaciogenic dust is assumed (Schroth et al., 2009), such that the global DFe flux is 24.5 Gmol year⁻¹. This value is approximately 10 times larger than that of the PI simulation and is larger than a recent estimation, suggesting that a quadrupling of the global DFe flux is constrained by a model–proxy comparison of δ¹⁵N and δ¹³C (Muglia et al., 2018). As with the present DFe input from dust, glacial DFe input has large uncertainties. As an upper estimate of the DFe flux from dust, we set the iron solubility at 10 % in glaciogenic dust in LGM_glac10%.

The DFe input flux from the sediments is estimated based on Moore and Braucher (2008). We assumed that the sedimentary DFe flux is proportional to the flux of organic carbon reaching the sea floor. To consider the realistic bathymetry of the continental shelves, the iron flux is weighted by the fraction of bottom area of the ETOPOV2 data that falls within the bounds of the model grid cell. The global DFe flux from the sediments in the PI is 33.1 Gmol year⁻¹. In the LGM simulations, the DFe input from sedimentary sources changes according to the flux of organic carbon reaching the sea floor. A decrease in the DFe input from sedimentary sources because of a sea-level drop is not considered. Muglia et al. (2017) showed this effect causes a CO₂ increase of 15 ppm. The hydrothermal DFe flux is regulated by the ridge spreading

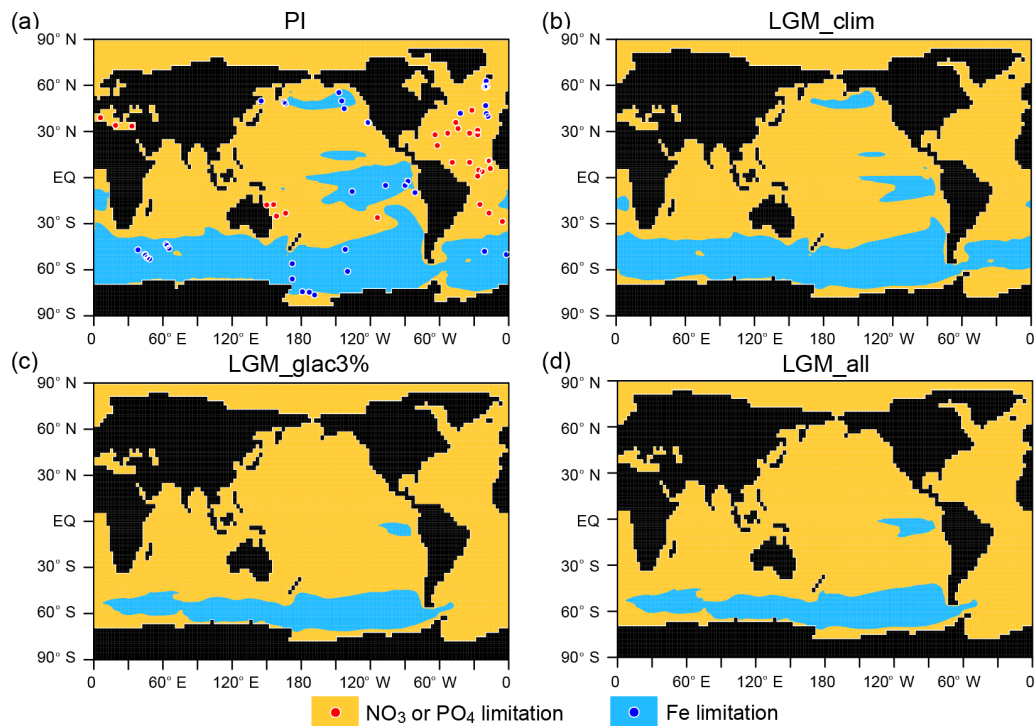


Figure 1. Primary limiting nutrient for phytoplankton for the (a) PI, (b) LGM_clim, (c) LGM_glac3%, and (d) LGM_all. Shade indicates NO₃ or PO₄ limitation (orange) and Fe limitation (blue). Circles represent observed limiting nutrients from nutrient addition experiments (Moore et al., 2013).

rate, as parameterized by a constant DFe/helium ratio (Tagliabue et al., 2010). The hydrothermal DFe flux in the PI is $\sim 8.5 \text{ Gmol year}^{-1}$. In the LGM simulations, the DFe input from hydrothermal sources is the same as that from PI.

The biogeochemical model was initialized from annual mean climatology data based on the World Ocean Atlas 2009 (WOA2009; Garcia et al., 2010a, b) for dissolved NO₃, PO₄, and O₂ and the Global Ocean Data Analysis Project (Key et al., 2004) for DIC and ALK. The initial DFe concentration is a constant value of 0.6 nM. For the spin-up, the last 50 years of data in the MIROC PI experiments were cyclically applied to the offline ocean biogeochemical model. The model was spun up for more than 3000 years with a prescribed atmospheric CO₂ concentration of 285 ppm to eliminate model drift in the global inventory of all tracers. Similar to Yamamoto et al. (2015), all physical and biogeochemical tracers, except salinity and dissolved iron, have correlation coefficients with observational data greater than 0.85 and normalized standard deviation values between 0.7 and 1.1.

LGM experiments were run for 3000 years, following 3000 years of spin-up under PI conditions. The atmospheric CO₂ concentration was predicted. We increased the salinity, PO₄, and NO₃ inventory by 3 % to account for the reduced ocean volume because of the sea-level drop. All experiments are listed in Table 1. LGM_clim uses LGM boundary conditions. LGM_dust is based on LGM_clim but uses

the dust deposition flux of LGMctl. Similarly, LGM_glac3% and LGM_glac10% use the dust deposition flux of LGMglac but with an iron solubility of glaciogenic dust of 3 % and 10 %, respectively. LGM_all is similar to LGM_glac3%, but the NO₃ and PO₄ inventories are increased by 15 %. This assumption is based on a recent model simulation that shows a $\sim 15 \%$ increase in nutrient inventory is caused by reduced organic matter burial in shallow sediments associated with a sea-level drop (Wallmann et al., 2016). In our simulations, changes in benthic denitrification were not considered. Somes et al. (2017) show that a decrease in benthic denitrification because of a sea-level drop reduces NO₃ loss and thus leads to a larger NO₃ inventory in the LGM ocean. We analyzed the results from the last 100 years of each simulation.

3 Results and discussion

3.1 Glacial nutrient cycles and export production

In the LGM_clim, which uses LGM climate boundary conditions, the NO₃ redistribution induced by weaker and shallower AMOC reduces nutrient supply from the deep ocean to the surface (Table 2 and Fig. 2). The NO₃ concentration in the euphotic zone decreases by 12 % and the global export production (EP) is reduced by $0.54 \text{ Pg C year}^{-1}$ compared to that of the PI simulation. Corresponding to the surface NO₃ decrease, significant EP decreases are found in the North

Atlantic and North Pacific (Figs. 3a and S2). However, the surface DFe concentration slightly changes. Because these changes in DFe and NO₃ decrease the iron-limited areas by 27 % (Fig. 1b), the simulated LGM climate tends to mitigate the impacts of iron fertilization on biological productivity and the carbon cycle.

To evaluate the impacts of desert and glaciogenic dust on the ocean biogeochemical cycles, we conducted sensitivity studies. The DFe input from desert dust with a 1 % iron solubility was applied in LGM_dust, whereas glaciogenic dust with 3 % or 10 % iron solubility was additionally applied in LGM_glac3% or LGM_glac10%, respectively. Iron fertilization from only desert dust has a limited impact on the EP. Iron fertilization from both desert and glaciogenic dust increases the EP by 0.88 Pg C year⁻¹ south of 45° S, whereas the EP decreases by 0.86 Pg C year⁻¹ north of 45° S, where most oceans are nitrogen-limited regions (LGM_glac3% – LGM_clim; Table 2). Enhanced primary production consumes the NO₃ of the euphotic zone in the SO and its anomaly is transported to the Antarctic bottom water (AABW). Subsequently, the surface NO₃ reduction in the SO is also transported to low-latitude regions via surface and intermediate waters (Fig. 2), thus reducing the EP in nitrogen-limited regions at low latitudes. Remarkable EP reductions occur north of the iron-limited regions of the SO (Fig. 3b). Our results demonstrate that enhanced biotic carbon export in the SO is partly compensated for by reduced carbon export in low-latitude regions. From the comparison between the effect of desert dust (LGM_dust – LGM_clim) and that of glaciogenic dust (LGM_glac3% – LGM_dust), we found that an increase in the EP due to dust-borne iron fertilization in the SO is mainly caused by glaciogenic dust (Table 2).

For 15 % increases in NO₃ and PO₄ inventory associated with sea-level drop (LGM_all), the EP increases globally in the nitrogen-limited regions, leading to a global EP increase of 0.86 Pg C year⁻¹ (LGM_all – LGM_glac3%; Table 2). Simulated EP changes from the PI are in good agreement with the paleo-productivity reconstruction (Kohfeld et al., 2013) (Fig. 3c). Among the common patterns is the north–south dipole pattern in the SO with an EP decrease at higher latitudes and an EP increase at lower latitudes. The EP decrease at higher latitudes is attributed to sea-ice expansion and the associated reduction of surface shortwave radiation (Oka et al., 2011), whereas iron fertilization increases the EP at lower latitudes. In the model, the EP changes also have an east–west dipole pattern; a slight EP increase is found in the South Pacific Ocean and significant EP increases occur in the South Atlantic and Indian oceans. We found that this pattern is attributed to iron fertilization by glaciogenic dust. Glaciogenic dust derived from Patagonian glaciers is transported to the South Atlantic and Indian oceans by the southern westerly wind; however, it is unable to reach the South Pacific (Fig. S3). Proxy data show no clear east–west dipole pattern, suggesting that the model underestimates iron fertilization in the Pacific sector of the Southern Ocean. However,

Table 2. Results of the model experiments. Simulated global average of surface NO₃, DFe, and Fe-limited area and changes in EP at 100 m, atmospheric CO₂, and globally averaged preformed PO₄, O₂, and apparent oxygen utilization (AOU) below 2000 m depth from the PI. Values in brackets are the PI results.

Experiments	Surface NO ₃ (mmol m ⁻³)	Surface DFe (μmol m ⁻³)	Fe-limited area (10 ⁶ km ²)	Global ΔEP (Pg C year ⁻¹)	ΔEP (> 45° S) (Pg C year ⁻¹)	ΔEP (< 45° S) (Pg C year ⁻¹)	Preformed PO ₄ (mmol m ⁻³)	ΔCO ₂ (ppm)	ΔO ₂ deep (mmol m ⁻³)	ΔAOUdeep (mmol m ⁻³)
PI	7.7	0.38	111	(8.54)	(6.19)	(2.35)	1.013	(285)	(156)	(182.5)
LGM_clim	6.8	0.39	81	-0.54	-0.45	-0.09	0.913	-26.4	-7	37.3
LGM_dust	6.9	0.42	80	-0.54	-0.49	-0.05	0.914	-27.6	-8	38.9
LGM_glac3%	5.8	0.5	35	-0.54	-1.31	+0.77	0.835	-43.2	-28	58.7
LGM_glac10%	5.5	0.54	23	-0.54	-1.46	+0.92	0.816	-46.4	-33	63.6
LGM_all	6.5	0.48	39	+0.32	-0.63	+0.95	1.002	-59.2	-42	72.8

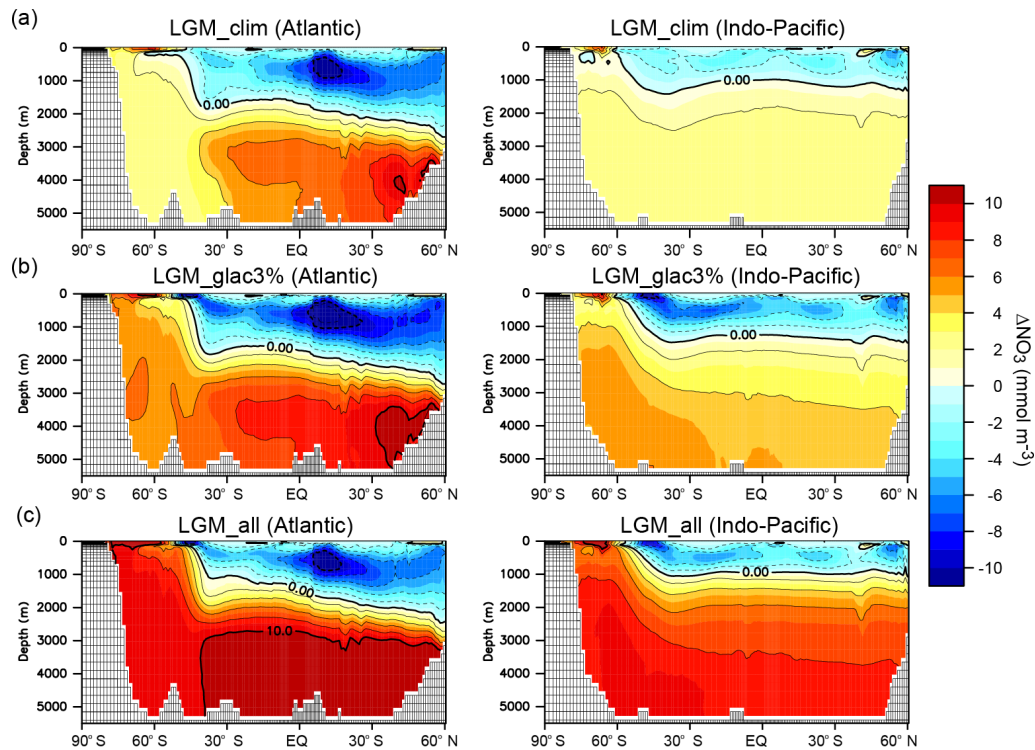


Figure 2. NO₃ change resulting from changes in the climate and biological pump in LGM simulations. Zonal mean changes in NO₃ from the PI to (a) LGM_clim, (b) LGM_glac3%, and (c) LGM_all. The left and right panels show the Atlantic and Indo-Pacific oceans, respectively.

proxy data in the South Pacific remain sparse and a quantitative comparison of EP changes between the South Atlantic and South Pacific is limited. Therefore, further proxy data in the South Pacific are required for a comprehensive understanding of the glacial EP changes and iron fertilization.

3.2 CO₂ reduction and its relationship to efficiency of the biological pump and dust flux

Climate change reduces the atmospheric CO₂ concentration by 26.4 ppm (LGM_clim – PI; Table 2), which is similar to that of previous simulations (Chikamoto et al., 2012; Menviel et al., 2012; Kobayashi et al., 2015). Circulation changes (i.e., a weaker and shallower AMOC and AABW expansion) cause DIC to decrease in the upper ocean and increase below 2000 m depth, such that the vertical DIC gradient between the surface and deep oceans is enhanced (Fig. 4). The efficiency of the oceanic biological pump is calculated following Ito and Follows (2005). The global mean preformed PO₄ is the difference between the total globally averaged PO₄ and global mean remineralized PO₄, $P_{\text{pref}} = P_{\text{tot}} - P_{\text{remi}}$. Here, P_{pref} is the preformed PO₄ concentration, P_{tot} is the total PO₄ concentration, and P_{remi} is the remineralized PO₄ concentration. The remineralized PO₄ is given by $P_{\text{remi}} = \text{AOU} \times R_{\text{P:O}}$, where $R_{\text{P:O}}$ is a constant phosphorous-to-oxygen ratio, and AOU is apparent oxygen utilization. A decrease in preformed PO₄, and thus an increase in remineralized PO₄,

indicates an increase in the efficiency of the oceanic biological pump. Although globally integrated EP decreases, circulation change and deepening of the remineralization profile due to seawater cooling (Matsumoto, 2007) reduce the preformed nutrient inventory, enhancing the efficiency of the biological pump (Table 2). The enhanced accumulation of respired carbon associated with the more efficient biological pump and increased CO₂ solubility from the lower SST contribute to a decreased CO₂. Notably, the AOU is different from true oxygen utilization due to the air–sea disequilibrium, which is on the order of 20 mmol m⁻³ in deep-water formation regions (Russell and Dickson, 2003; Duteil et al., 2013). Changes in surface ocean disequilibrium between the PI and LGM simulations might lead to large errors in the AOU changes (Khawala et al., 2019).

Iron fertilization from desert and glaciogenic dust enhances the vertical DIC gradient and causes a CO₂ reduction of 1.2 ppm (LGM_dust – LGM_clim) and 15.6 ppm (LGM_glac3% – LGM_dust), respectively. Our results show that the glacial CO₂ reduction due to dust-borne iron fertilization is mainly driven by glaciogenic dust. A simulated total CO₂ reduction of 16.8 ppm induced by iron fertilization is within the range of previous studies using OGCM or Earth system models of intermediate complexity (EMICs): 8–25 ppm CO₂ drawdown (Bopp et al., 2003; Parekh et al., 2006; Tagliabue et al., 2009; Oka et al., 2011; Menviel et al., 2012; Lambert et al., 2015; Heinze et al., 2016; Muglia et al.,

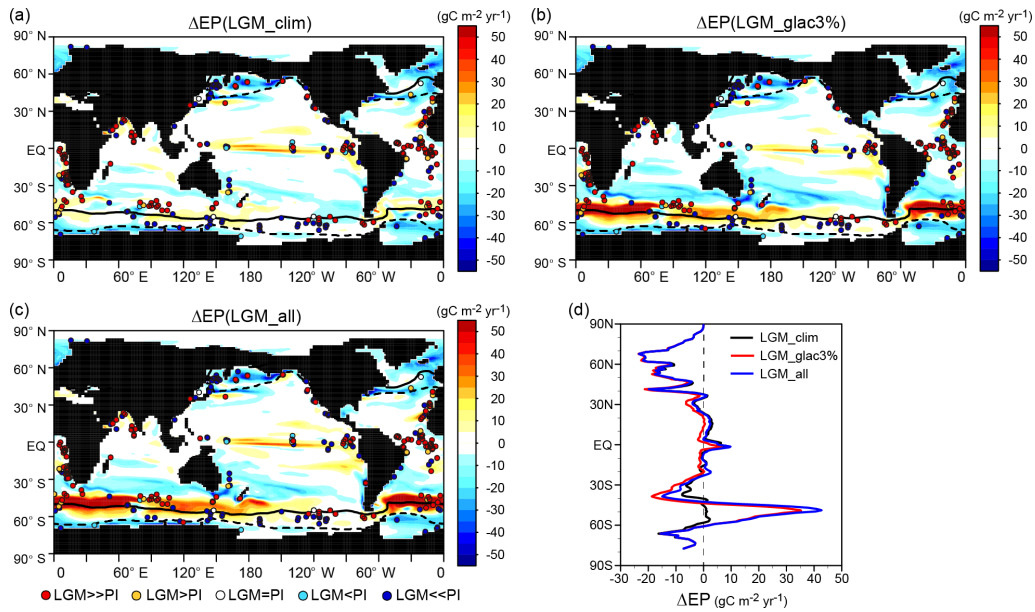


Figure 3. Model–proxy comparison of EP change from the PI to LGM. The EP difference from the PI for (a) LGM_clim, (b) LGM_glac3%, and (c) LGM_all. Circles show proxy data (Kohfeld et al., 2013). Solid (dotted) lines refer to the glacial sea-ice fraction of 0.1 during August (February). (d) Zonal mean changes in the surface EP from the PI for LGM_clim (black), LGM_glac3% (red), and LGM_all (blue).

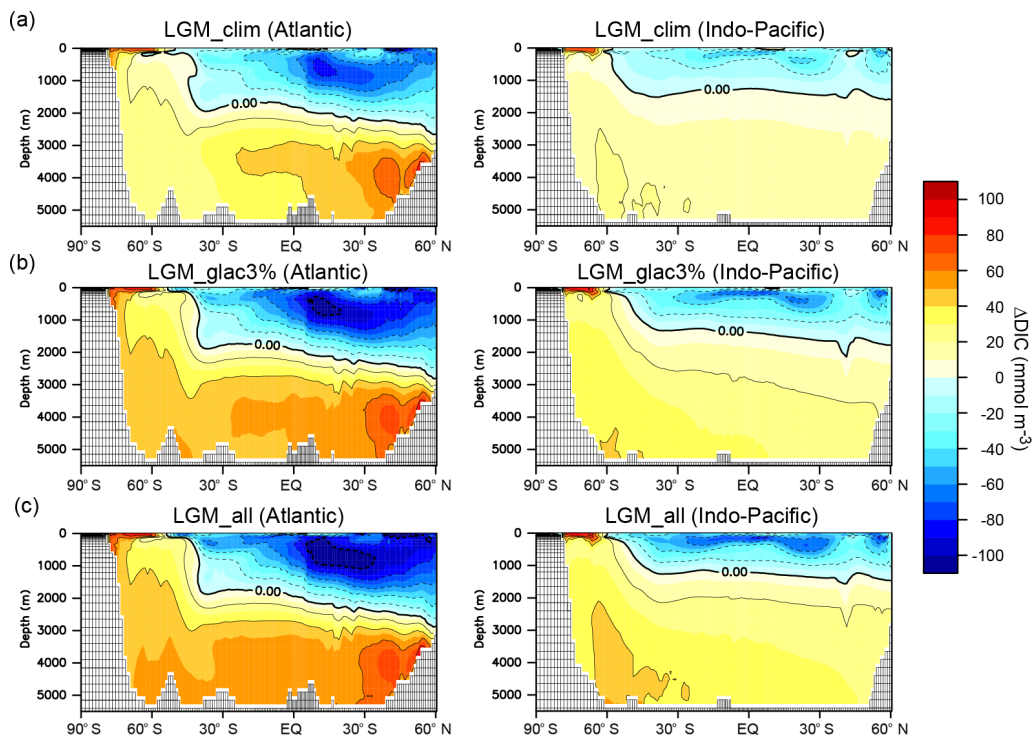


Figure 4. DIC change resulting from changes in the climate and biological pump in LGM simulations. Zonal mean changes in DIC from PI to (a) LGM_clim, (b) LGM_glac3%, and (c) LGM_all. The left and right panels show the Atlantic and Indo-Pacific oceans, respectively.

2017). DFe supply from dust also contributes to the glacial CO₂ reduction through enhanced efficiency of the biological pump (Table 2). The simulated atmospheric CO₂ concentration is proportionally reduced to the preformed PO₄ (Fig. 5a), similar to previous simulations under the present climate (Ito and Follows, 2005; Marinov et al., 2008). Figure 5b shows the CO₂ change in response to the DFe input magnitude. The iron fertilization efficiency to reduce CO₂ decreases with increasing DFe flux. This nonlinear response is driven by a decrease in the iron-limited areas and the associated weakening of the iron fertilization effect on EP (Fig. 5c). Because the iron-limited region dramatically decreases in size and the CO₂ difference between LGM_glac3% and LGM_glac10% is small, the CO₂ reduction of 20 ppm in LGM_glac10% is near the upper limit (i.e., there are no iron-limited regions and thus no additional CO₂ reduction).

The simulated upper limit of CO₂ reduction resulting from iron fertilization is not a robust result because present iron models have large uncertainty. While Parekh et al. (2008) show an upper limit of 10 ppm, other simulations show CO₂ decrease by greater than 20 ppm (Oka et al., 2011; Muglia et al., 2017). To obtain a better understanding of the impact of iron fertilization on glacial CO₂ decrease, the variability of the upper limit among iron models should be investigated in a future study.

Increases in nutrient inventory from lower sea levels drive an additional CO₂ drawdown by 16 ppm (LGM_all – LGM_glac3%). We found that changes in the biological pump induced by iron fertilization and an increase in nutrient inventory contribute to a glacial CO₂ decrease of more than 30 ppm. The resultant total CO₂ reduction is ~ 60 ppm, which our model does not reproduce as the full variation in the glacial–interglacial CO₂ change. Note that changes in the sedimentation process (i.e., carbonate compensation and burial–nutrient feedback) are not considered in our simulation. The simulated increase in the bottom water DIC (Fig. 4) would enhance calcium carbonate dissolution in the sediments and thereby increase ocean alkalinity, leading to a further CO₂ decrease (Bouttes et al., 2011; Brovkin et al., 2012; Kobayashi and Oka, 2018). The long-term balance between the burial of organic material and nutrient input through weathering is also potentially important for the atmospheric CO₂ response (Roth et al., 2014; Wallmann et al., 2016). For example, Tschumi et al. (2011) show that the nutrient–burial feedback significantly amplifies the effect of an increase in the PO₄ inventory on the glacial CO₂ decrease. Menviel et al. (2012) quantified the implication of ocean–sediment–lithosphere coupling for factorial experiments with an altered iron fertilization and altered PO₄ inventory from transient glacial–interglacial simulations. Considering that EP increases due to iron fertilization and the nutrient increase are smaller in our simulations than that in previous studies (Tschumi et al., 2011; Menviel et al., 2012), the effect of burial–nutrient feedback on the glacial CO₂ reduction may be smaller than previously estimated. As described

in the next section, to assess the simulated accumulation of respired carbon, we compared the simulated oxygen changes to qualitative and quantitative proxy records.

3.3 Model–proxy comparison of glacial oxygen changes

Compared to the compilation of qualitative and quantitative proxy records of oxygen change from the Holocene to Last Glacial Maximum, LGM_clim shows an increase in oxygen for the entire SO and underestimates deoxygenation in the deep Pacific and Indian oceans, in contrast to the proxy records (Fig. 6a). However, LGM_all successfully reproduces large-scale spatial patterns of oxygen change, including for the SO (Fig. 6b). Moreover, the simulated changes in oxygen concentration agree well with quantitative reconstructions: a 45–65 mmol m⁻³ decrease in the deep North Atlantic (Hoogakker et al., 2015), an ~ 30–80 mmol m⁻³ decrease in the eastern equatorial Pacific (Hoogakker et al., 2018; Umling and Thunell, 2018), and a > 80 mmol m⁻³ in the upper SO of the Pacific sector (Lu et al., 2016). Our results clearly show the importance of iron fertilization and an increase in nutrient inventory in global deep deoxygenation. These model–proxy agreements of oxygen change support the simulated CO₂ decrease of 30 ppm by the biological pump. However, the reconstructed O₂ decrease of ~ 175 mmol m⁻³ in the deep SO (Gottschalk et al., 2016) is much greater than the simulated decrease of ~ 30 mmol m⁻³ from LGM_all; thus, the respired carbon accumulation in the deep SO is underestimated in our model. This may be one of the reasons why the glacial–interglacial CO₂ change of ~ 100 ppm cannot be reproduced in our simulations.

To clarify the mechanism of O₂ change from LGM_all to PI, we decomposed the O₂ change into changes in saturation (O_{2sat}) and apparent oxygen utilization (AOU), where $\Delta O_2 = \Delta O_{2sat} - \Delta AOU$. O_{2sat} is computed from simulated seawater temperature and salinity and AOU by subtracting the O₂ concentration from O_{2sat}. Ocean cooling increases O_{2sat} globally, increasing the global mean value by 25.5 mmol m⁻³ (Fig. 7a). As with the O₂ change, ΔAOU shows a contrast between the upper and deep oceans (Fig. 7b). At a depth of 0–800 m, the AOU decreases by 5.2 mmol m⁻³ north of 45° S, which results from the decrease in biological oxygen consumption associated with EP reduction and increased ventilation (Fig. 7f). Therefore, the combined effects of an O_{2sat} increase and AOU decrease contribute to an overall O₂ increase in the upper ocean. In the deep ocean (> 2 km depth), the sum of AOU increases by 72.8 mmol m⁻³ (LGM_all in Table 2), overcoming the O_{2sat} increase, resulting in deep O₂ depletion. The relationships between changes in the O₂ concentration, O_{2sat}, and AOU are consistent with that of a previous simulation (Bopp et al., 2017).

The ΔAOU is also decomposed into effects of climate change (LGM_clim – PI), iron fertilization (LGM_glac3% – LGM_clim), and an increase in nutrient inventory (LGM_all

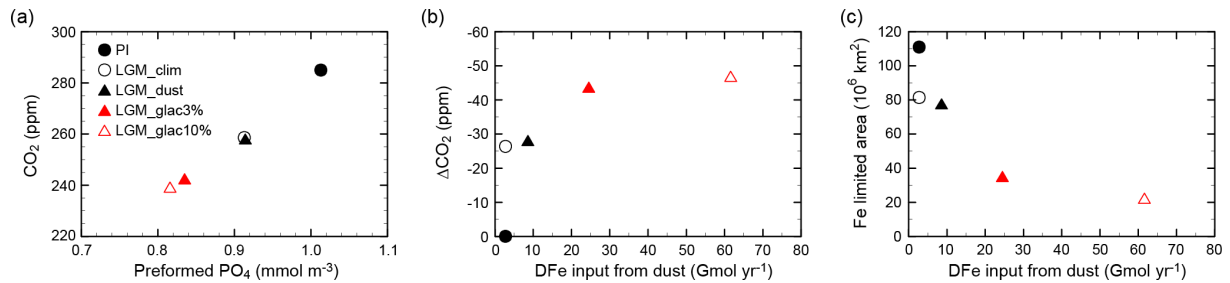


Figure 5. CO₂ change and its relationship to efficiency of the biological pump and iron cycle. (a) Atmospheric CO₂ as a function of globally averaged preformed PO₄. (b) Changes in CO₂ from the PI as a function of DFe input from dust. (c) Fe-limited area as a function of DFe input from dust. Shown are the PI (black filled circle), LGM_clim (black open circle), LGM_dust (black filled triangle), LGM_glac3% (red filled triangle), and LGM_glac10% (red open triangle).

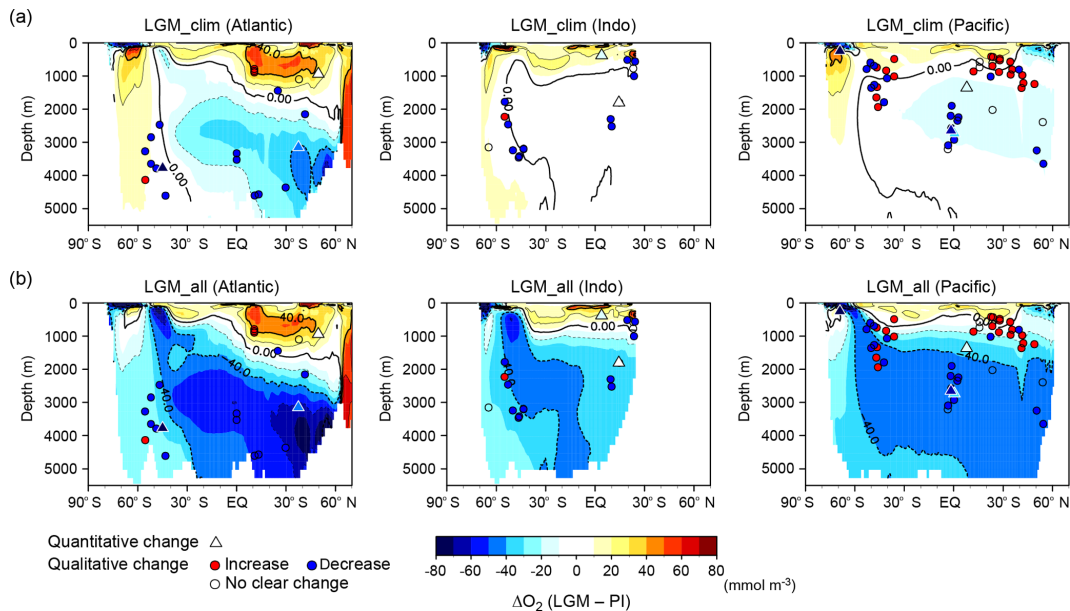


Figure 6. Model–proxy comparison of changes in dissolved oxygen concentration from the PI to LGM. Zonal mean changes in O₂ from the PI to (a) LGM_clim and (b) LGM_all for the Atlantic (left), Indian (middle), and Pacific (right) oceans; the contour interval is 20 mmol m⁻³. Circles show proxy records of qualitative O₂ change from multi-proxy data compilation from Jaccard and Galbraith (2012) (except δ¹⁵N data), Jaccard et al. (2016), and Durand et al. (2018). Red (blue) circles indicate O₂ increase (decrease) from the Holocene to LGM. Triangles show proxy records of quantitative O₂ change (Schmiedl and Mackensen, 2006; Hoogakker et al., 2015, 2018; Gottschalk et al., 2016; Lu et al., 2016; Bunzel et al., 2017; Umling and Thunell, 2018) (triangles shaded using the same color scale).

– LGM_glac3%). The effects of climate change, circulation change, restricted air–sea gas exchange from sea-ice expansion, and deepening of remineralization due to seawater cooling lead to the AOU increasing by 37.3 mmol m⁻³ in the deep ocean (Table 2). In the deep North Atlantic, the simulated water mass age is older in the LGM than in the PI by up to 500 years, suggesting reduced ventilation (Fig. 7f). Therefore, significant AOU increases occur (Fig. 7c). Meanwhile, in the SO and deep Pacific Ocean, an increase in ventilation tends to decrease the AOU and thus partly compensates for the increase in the AOU. Regarding the effects of iron fertilization and nutrient inventory, the EP changes associated with iron fertilization and an increase in nutrient inventory

enhance biological oxygen consumption and thus increase the AOU by 21.4 and 14.1 mmol m⁻³ in the deep ocean, respectively (Table 2 and Fig. 7d, e). In particular, glaciogenic dust causes an increase in the AOU of 19.8 mmol m⁻³. Our results demonstrate that in addition to climate change, enhanced biological oxygen consumption associated with iron fertilization and increased nutrient inventory are crucial drivers of glacial deoxygenation in the deep ocean. While some previous modeling studies show deep-ocean oxygenation during the LGM (Buchanan et al., 2016; Galbraith and Laverne, 2019), this study and others reproduce deep-ocean deoxygenation (Galbraith and Jaccard, 2015; Schmittner and Somes, 2016; Bopp et al., 2017; Somes et al., 2017). The

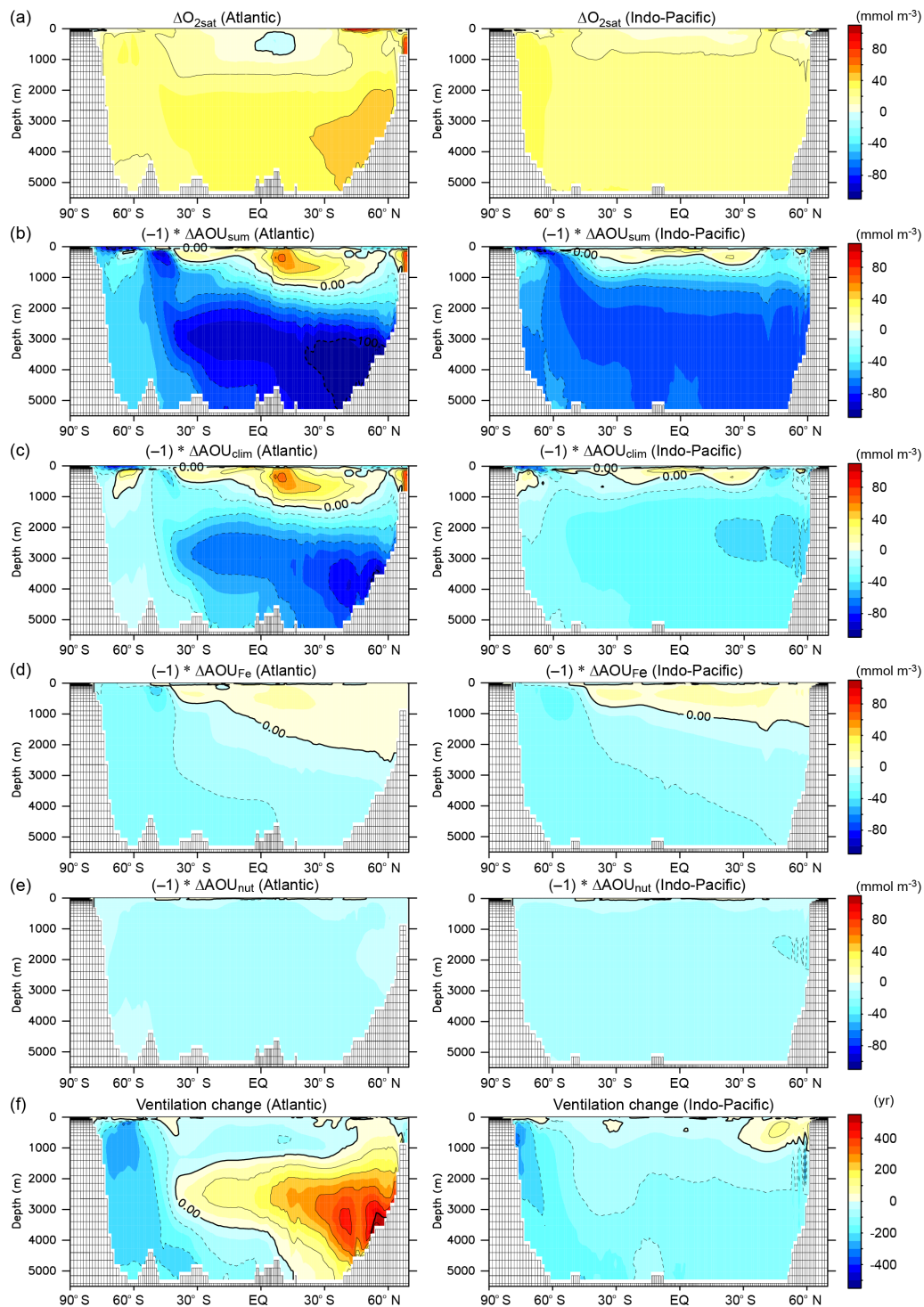


Figure 7. Contributions of individual mechanisms to oxygen change and ventilation change. Zonal mean changes of (a) O_{2sat} , (b) AOU_{sum} , (c) AOU_{clim} , (d) AOU_{Fe} , (e) AOU_{nut} , and (f) ventilation age from the PI to LGM. Left and right panels show the Atlantic and Indo-Pacific oceans: the contour intervals are 20 mmol m^{-3} for panels (a)–(e) and 100 years for panel (f). We decomposed the total AOU change ($\Delta AOU_{sum} = AOU_{(LGM_all)} - AOU_{(PI)}$) into the effects of climate change ($\Delta AOU_{clim} = AOU_{(LGM_clim)} - AOU_{(PI)}$), iron fertilization ($\Delta AOU_{Fe} = AOU_{(LGM_glac3\%)} - AOU_{(LGM_clim)}$), and nutrient inventory increase ($\Delta AOU_{nut} = AOU_{(LGM_all)} - AOU_{(LGM_glac3\%)}$).

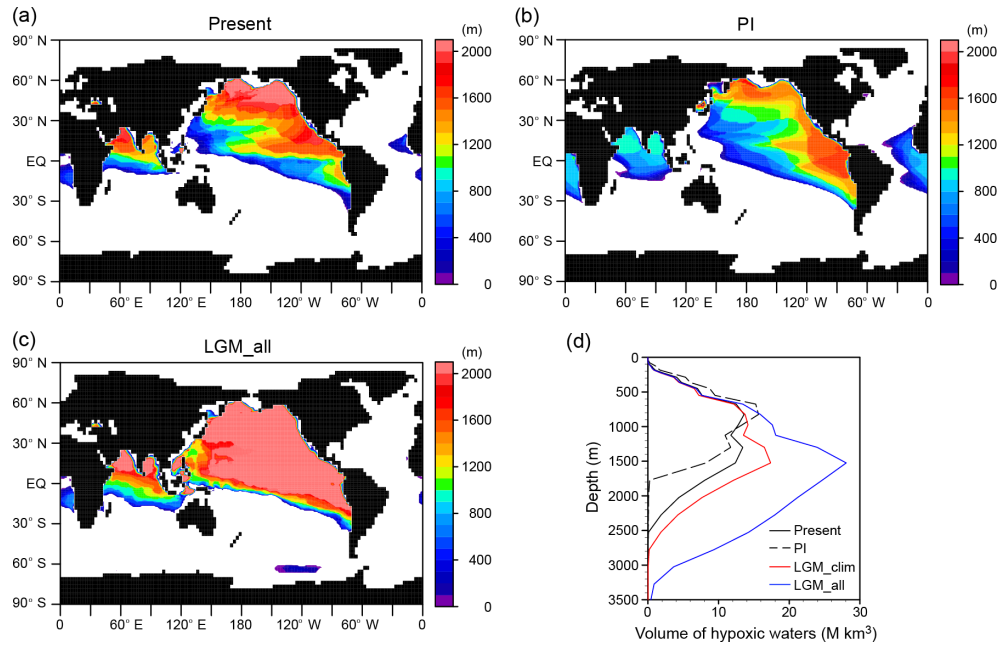


Figure 8. Hypoxic waters expansion. Horizontal distribution of thickness of the hypoxic waters ($[O_2] < 80 \text{ mmol m}^{-3}$) for the (a) present, (b) PI, and (c) LGM_all. (d) Vertical distribution of hypoxic waters for the present (black solid), PI (black dashed), LGM_clim (red), and LGM_all (blue). Because current coarse resolution models have difficulties reproducing low oxygen concentration for the present day (Bopp et al., 2013), observed values from WOA2009 (Garcia et al., 2010a) were used for the present. For the LGM simulations, we combined the observed values with the modeled changes.

conflicting oxygen change between the previous simulations can be attributed to different treatments of enhanced biological oxygen consumption because iron fertilization and increased nutrient inventory are not considered in these simulations that fail to reproduce deep deoxygenation (Buchanan et al., 2016; Galbraith and Lavergne, 2019).

Glacial oxygen change expands the volume of hypoxic waters (defined here as $[O_2] < 80 \text{ mmol m}^{-3}$) below 1000 m depth, such that the simulated global volume increases from the present value of 120 to 237 Mkm³ in LGM_all. Significant expansion occurs in the deep Pacific and Indian oceans (Fig. 8), with hypoxic waters also appearing in the upper SO in the Pacific sector, consistent with proxy records (Hoogakker et al., 2018; Lu et al., 2016). Because hypoxic conditions are lethal for more than one-half of marine benthic animals (Vaquer-Sunyer and Duarte, 2008), expansion of hypoxic water in the deep ocean can have an adverse impact on benthic fauna. Determining the biotic responses to glacial expansion of hypoxic water would be helpful for understanding the biotic response to future deoxygenation associated with global warming.

Finally, we discuss the underestimation of deoxygenation in the deep SO in LGM_all. Because simulated changes in the biological pump and sea-ice distributions are consistent with reconstructions (Obase et al., 2017), we then addressed circulation changes. The simulated water mass age of the deep SO is younger during the LGM than during the PI

by ~ 200 years (Fig. 7f), indicating an increase in ventilation. However, $\Delta^{14}\text{C}$ records show an increase in water mass age of more than 1000 years and thus increased stratification (Skinner et al., 2010; Burke and Robinson, 2012). Enhanced mixing of surface waters with deep waters supplies oxygen-rich surface waters to the deep ocean and simultaneously releases carbon accumulated in the deep water to the atmosphere. Therefore, we attribute the underestimation of deoxygenation and carbon accumulation in the deep SO to overestimated ventilation. Our results suggest that a stratified SO is required for reproducing glacial CO₂ drawdown and oxygen decline in the deep SO, consistent with recent paleo-proxy data and models (Fischer et al., 2010; Sigman et al., 2010; Kobayashi et al., 2015; Menviel et al., 2017). Menviel et al. (2017) showed that weaker and shallower North Atlantic Deep Water and weaker AABW could be necessary to reproduce the LGM oceanic $\delta^{13}\text{C}$ and radiocarbon distribution.

4 Conclusion and remarks

We quantified the impacts on glacial deoxygenation and CO₂ decreases caused by glaciogenic dust with higher iron solubility and increase in nutrient inventory associated with a sea-level drop using the coupled atmosphere–ocean general circulation model, aerosol model, and ocean biogeochemical model. As a result, we successfully reproduced the magni-

tude and large-scale pattern of the observed oxygen change between the present and LGM. Our results show that iron fertilization from glaciogenic dust and an increase in nutrient inventory could explain a glacial CO₂ decline of more than 30 ppm and approximately one-half of deep-ocean deoxygenation. These results also demonstrate the usefulness of the quantitative model–proxy comparison of oxygen change in understanding glacial–interglacial CO₂ change. However, large uncertainty remains because of the limited number of proxy data of quantitative oxygen change. Thus, we anticipate our findings will encourage studies to obtain further qualitative and quantitative reconstructions from throughout the global deep ocean. A comparison between the models and other proxy data (e.g., $\delta^{13}\text{C}$; Schmittner and Somes, 2016) is also required to obtain a more robust and comprehensive understanding of the glacial carbon cycle.

The changes in nutrient inventory during the LGM have large uncertainties. Previous studies estimate that the oceanic PO₄ and NO₃ inventories could have been 15 %–40 % (Tamburini and Föllmi, 2009; Wallmann et al., 2016) and 10 %–100 % (Deutsch et al., 2004; Eugster et al., 2013; Somes et al., 2017) greater during glacial compared to interglacial periods, respectively. Moreover, Somes et al. (2017) shows that sedimentary $\delta^{15}\text{N}$ records provide no constraint on this effect. Future simulations should test the biogeochemical sensitivity to nutrient inventory changes.

We focused on the impacts of DFe flux changes from the dust on glacial CO₂ drawdown and deoxygenation in this study. However, changes in the sedimentary and hydrothermal DFe flux and ligand concentration that are not considered in this study could also be important. A glacial sea-level drop decreases the sedimentary DFe flux due to the continental shelf reduction. However, the hydrothermal DFe flux is increased by the lower sea level and bottom pressure (Middleton et al., 2016). Muglia et al. (2017) show that the changes in sedimentary and hydrothermal DFe flux associated with a sea-level drop increase CO₂ by 15 ppm and decrease CO₂ by 6 ppm, respectively. Although sedimentary DFe flux is proportional to the organic carbon flux reaching the seafloor in our model, a parameterization with the DFe flux as a function of organic carbon flux and bottom oxygen concentrations is proposed in Dale et al. (2015). Glacial deep-water deoxygenation would increase sedimentary DFe flux, leading to a further CO₂ decrease via the biological pump. Ligand concentrations strongly control DFe concentrations (Gledhill and Buck, 2012). Because the ligand concentration is affected by numerous factors (Völker and Tagliabue, 2015), changes in ligand concentration from the PI to LGM have large uncertainty. Thus, we quantified the effect of DFe flux changes under a constant ligand concentration in the PI and LGM simulations. Changes in the sedimentary and hydrothermal DFe flux and ligand concentration should be the subject of future research.

Our model–proxy comparison shows the importance of the combination of a more sluggish SO circulation and enhanced

biological transport of organic matter in the increased accumulation of respired carbon and deoxygenation in the deep SO. However, present climate models cannot reproduce the stratified SO. A possible reason is that they are too coarse to capture the process of dense water formation on the Antarctic shelf and tend to underestimate the strength of stratification in the SO (Heuzé et al., 2013). The brine rejection process and/or change in the vertical diffusion coefficient could be necessary to reproduce the stratified SO (Kobayashi et al., 2015; Bouttes et al., 2011). Similar to glacial oxygen changes, changes in ocean circulation in the SO are crucial in projecting future oxygen changes associated with global warming (Yamamoto et al., 2015). Therefore, an understanding of glacial oxygen changes will aid in better understanding and predicting future oxygen changes.

Data availability. Data are freely available from the corresponding author (akitomo@jamstec.go.jp) upon request.

Supplement. The supplement related to this article is available online at: <https://doi.org/10.5194/cp-15-981-2019-supplement>.

Author contributions. AY and AAO designed the research. AY conducted and analyzed experiments and prepared the paper. AAO provided the results of MIROC. RO provided the results of MIROC-ESM. All authors discussed the results and gave their input on the manuscript.

Competing interests. The authors declare that they have no conflict of interest.

Special issue statement. This article is part of the special issue “Ocean deoxygenation: drivers and consequences – past, present and future (BG/CP/OS inter-journal SI)”. It is a result of the International Conference on Ocean Deoxygenation, Kiel, Germany, 3–7 September 2018.

Acknowledgements. We thank the Editor Laurie Menviel as well as Fortunat Joos and Andreas Schmittner for their helpful comments. This work was supported by the Integrated Research Program for Advancing Climate Models (TOUGOU program) from the Ministry of Education, Culture, Sports, Science and Technology (MEXT), Japan, and JSPS KAKENHI grant no. JP17H06323 and JP17H06104. The simulations with the offline biogeochemical model were performed using the Fujitsu PRIMEHPC FX10 system in the Information Technology Center, University of Tokyo.

Financial support. This work was supported by the Integrated Research Program for Advancing Climate Models (TOUGOU program) from the Ministry of Education, Culture, Sports, Science

and Technology (MEXT), Japan, and the Japan Society for the Promotion of Science (JSPS) KAKENHI under grant numbers JP17H06323 and JP17H06104.

Review statement. This paper was edited by Laurie Menviel and reviewed by Andreas Schmittner and Fortunat Joos.

References

- Albani, S., Mahowald, N. M., Perry, A. T., Scanza, R. A., Zender, C. S., Heavens, N. G., Maggi, V., Kok, J. F., and Otto-Bliesner, B. L.: Improved dust representation in the Community Atmosphere Model., *J. Adv. Model. Earth Sy.*, 6, 541–570, <https://doi.org/10.1002/2013ms000279>, 2014.
- Bopp, L., Kohfeld, K. E., and Le Quéré, C.: Dust impact on marine biota and atmospheric CO₂ during glacial periods, *Paleoceanography*, 18, 1046, <https://doi.org/10.1029/2002PA000810>, 2003.
- Bopp, L., Resplandy, L., Orr, J. C., Doney, S. C., Dunne, J. P., Gehlen, M., Halloran, P., Heinze, C., Ilyina, T., Séférian, R., Tjiputra, J., and Vichi, M.: Multiple stressors of ocean ecosystems in the 21st century: projections with CMIP5 models, *Biogeosciences*, 10, 6225–6245, <https://doi.org/10.5194/bg-10-6225-2013>, 2013.
- Bopp, L., Resplandy, L., Untersee, A., Le Mezo, P., and Kageyama, M.: Ocean (de)oxygenation from the Last Glacial Maximum to the twenty-first century: insights from Earth System models, *Philos. T. R. Soc. S.-A*, 375, 2102, <https://doi.org/10.1098/rsta.2016.0323>, 2017.
- Bouttes, N., Paillard, D., Roche, D. M., Brovkin, V., and Bopp, L.: Last Glacial Maximum CO₂ and $\delta^{13}\text{C}$ successfully reconciled, *Geophys. Res. Lett.*, 38, L02705, <https://doi.org/10.1029/2010gl044499>, 2011.
- Braconnot, P., Otto-Bliesner, B., Harrison, S., Joussaume, S., Peterchmitt, J.-Y., Abe-Ouchi, A., Crucifix, M., Driesschaert, E., Fichefet, Th., Hewitt, C. D., Kageyama, M., Kitoh, A., Laîné, A., Loutre, M.-F., Marti, O., Merkel, U., Ramstein, G., Valdes, P., Weber, S. L., Yu, Y., and Zhao, Y.: Results of PMIP2 coupled simulations of the Mid-Holocene and Last Glacial Maximum – Part 1: experiments and large-scale features, *Clim. Past*, 3, 261–277, <https://doi.org/10.5194/cp-3-261-2007>, 2007.
- Broecker, W. S.: Glacial to interglacial changes in ocean chemistry, *Prog. Oceanogr.*, 11, 151–197, [https://doi.org/10.1016/0079-6611\(82\)90007-6](https://doi.org/10.1016/0079-6611(82)90007-6), 1982.
- Brovkin, V., Ganopolski, A., Archer, D., and Munhoven, G.: Glacial CO₂ cycle as a succession of key physical and biogeochemical processes, *Clim. Past*, 8, 251–264, <https://doi.org/10.5194/cp-8-251-2012>, 2012.
- Buchanan, P. J., Matear, R. J., Lenton, A., Phipps, S. J., Chase, Z., and Etheridge, D. M.: The simulated climate of the Last Glacial Maximum and insights into the global marine carbon cycle, *Clim. Past*, 12, 2271–2295, <https://doi.org/10.5194/cp-12-2271-2016>, 2016.
- Bunzel, D., Schmiedl, G., Lindhorst, S., Mackensen, A., Reolid, J., Romahn, S., and Betzler, C.: A multi-proxy analysis of Late Quaternary ocean and climate variability for the Maldives, Inner Sea, *Clim. Past*, 13, 1791–1813, <https://doi.org/10.5194/cp-13-1791-2017>, 2017.
- Burke, A. and Robinson, L. F.: The Southern Ocean’s role in carbon exchange during the last deglaciation, *Science*, 335, 557–561, 2012.
- Chikamoto, M. O., Abe-Ouchi, A., Oka, A., Ohgaito, R., and Timmermann, A.: Quantifying the ocean’s role in glacial CO₂ reductions, *Clim. Past*, 8, 545–563, <https://doi.org/10.5194/cp-8-545-2012>, 2012.
- Ciais, P., Sabine, C., Bala, G., Bopp, L., Brovkin, V., Canadell, J., Chhabra, A., DeFries, R., Galloway, J., Heimann, M., Jones, C., Le Quéré, C., Myneni, R. B., Piao, S., and Thornton, P.: Carbon and Other Biogeochemical Cycles, in: *Climate Change 2013: The Physical Science Basis. Contribution of Working Group I to the Fifth Assessment Report of the Intergovernmental Panel on Climate Change*, edited by: Stocker, T. F., Qin, D., Plattner, G.-K., Tignor, M., Allen, S. K., Boschung, J., Nauels, A., Xia, Y., Bex, V., and Midgley, P. M., Cambridge University Press, Cambridge, UK and New York, NY, USA, 465–570, 2013.
- Conway, T., Wolff, E., Roethlisberger, R., Mulvaney, R., and Elderfield, H.: Constraints on soluble aerosol iron flux to the Southern Ocean at the Last Glacial Maximum, *Nat. Commun.*, 6, 1–9, <https://doi.org/10.1038/ncomms8850>, 2015.
- Curry, W. B. and Oppo, D. W.: Glacial water mass geometry and the distribution of $\delta^{13}\text{C}$ of CO₂ in the western Atlantic Ocean, *Paleoceanography*, 20, PA1017, <https://doi.org/10.1029/2004PA001021>, 2005.
- Dale, A. W., Nickelsen, L., Scholz, F., Hensen, C., Oschlies, A., and Wallmann, K.: A revised global estimate of dissolved iron fluxes from marine sediments, *Global Biogeochem. Cy.*, 29, 691–707, <https://doi.org/10.1002/2014GB005017>, 2015.
- Deutsch, C., Sigman, D. M., Thunell, R. C., Meckler, A. N., and Haug, G. H.: Isotopic constraints on glacial/interglacial changes in the oceanic nitrogen budget, *Global Biogeochem. Cy.*, 18, GB4012, <https://doi.org/10.1029/2003GB002189>, 2004.
- Durand, A., Chase, Z., Noble, T. L., Bostock, H., Jaccard, S. L., Townsend, A. T., Bindoff, N. L., Neil, H., and Jacobsen, G.: Reduced oxygenation at intermediate depth of the southwest Pacific during the last glacial maximum, *Earth Planet. Sc. Lett.*, 491, 48–57, 2018.
- Duteil, O., Koeve, W., Oschlies, A., Bianchi, D., Galbraith, E., Kriest, I., and Matear, R.: A novel estimate of ocean oxygen utilisation points to a reduced rate of respiration in the ocean interior, *Biogeosciences*, 10, 7723–7738, <https://doi.org/10.5194/bg-10-7723-2013>, 2013.
- Eppley, R. W.: Temperature and phytoplankton growth in the sea, *Fish. B.-NOAA*, 70, 1063–1085, 1972.
- Eugster, O., Gruber, N., Deutsch, C., Jaccard, S. L., and Payne, M. R.: The dynamics of the marine nitrogen cycle across the last deglaciation, *Paleoceanography*, 28, 116–129, <https://doi.org/10.1002/palo.20020>, 2013.
- Fischer, H., Schmitt, J., Luthi, D., Stocker, T. F., Tschumi, T., Parekh, P., Joos, F., Kohler, P., Volker, C., Gersonde, R., Barbante, C., Le Floch, M., Raynaud, D., and Wolff, E.: The role of Southern Ocean processes in orbital and millennial CO₂ variations – a synthesis, *Quaternary Sci. Rev.*, 29, 193–205, 2010.
- Galbraith, E. and de Lavergne, C.: Response of a comprehensive climate model to a broad range of external forcings: relevance for deep ocean ventilation and the development of late Cenozoic ice ages, *Clim. Dynam.*, 52, 653–679, <https://doi.org/10.1007/s00382-018-4157-8>, 2019.

- Galbraith, E. D. and Jaccard, S. L.: Deglacial weakening of the oceanic soft tissue pump: global constraints from sedimentary nitrogen isotopes and oxygenation proxies, *Quaternary Sci. Rev.*, 109, 38–48, <https://doi.org/10.1016/j.quascirev.2014.11.012>, 2015.
- Garcia, H. E., Locarnini, R., Boyer, T., Antonov, J., Baranova, O., Zweng, M., and Johnson, D.: Volume 3: Dissolved Oxygen, Apparent Oxygen Utilization, and Oxygen Saturation, *World Ocean Atlas 2009*, S. Levitus, Ed. NOAA Atlas NESDIS 70, US Government Printing Office, Washington, DC, 344 pp., 2010a.
- Garcia, H. E., Locarnini, R., Boyer, T., Antonov, J., Zweng, M., Baranova, O., and Johnson, D.: Volume 4: Nutrients (phosphate, nitrate, silicate), *World Ocean Atlas 2009*, S. Levitus, Ed., NOAA Atlas NESDIS 71, US Government Printing Office, Washington, DC, 398 pp., 2010b.
- Gledhill, M. and Buck, K.: The organic complexation of iron in the marine environment: a review, *Front. Microbiol.*, 3, 1–17, <https://doi.org/10.3389/fmicb.2012.00069>, 2012.
- Gottschalk, J., Skinner, L. C., Lippold, J., Vogel, H., Frank, N., Jaccard, S. L., and Waelbroeck, C.: Biological and physical controls in the Southern Ocean on past millennial-scale atmospheric CO₂ changes, *Nat. Commun.*, 7, 11539, <https://doi.org/10.1038/ncomms11539>, 2016.
- Heinze, C., Hoogakker, B. A. A., and Winguth, A.: Ocean carbon cycling during the past 130 000 years – a pilot study on inverse palaeoclimate record modelling, *Clim. Past*, 12, 1949–1978, <https://doi.org/10.5194/cp-12-1949-2016>, 2016.
- Heuzé, C., Heywood, K. J., Stevens, D. P., and Ridley, J. K.: Southern Ocean bottom water characteristics in CMIP5 models, *Geophys. Res. Lett.*, 40, 1409–1414, <https://doi.org/10.1002/grl.50287>, 2013.
- Hoogakker, B. A. A., Elderfield, H., Schmiedl, G., McCave, I. N., and Rickaby, R. E. M.: Glacial–interglacial changes in bottom water oxygen content on the Portuguese margin, *Nat. Geosci.*, 8, 40–43, <https://doi.org/10.1038/ngeo2317>, 2015.
- Hoogakker, B. A. A., Lu, Z., Umling, N., Jones, L., Zhou, X., Rickaby, R. E. M., Thunell, R., Cartapanis, O., and Galbraith, E.: Glacial expansion of oxygen-depleted seawater in the eastern tropical Pacific, *Nature*, 562, 410–413, <https://doi.org/10.1038/s41586-018-0589-x>, 2018.
- Ito, A., Myriokefalitakis, S., Kanakidou, M., Mahowald, N. M., Scanza, R. A., Hamilton, D. S., Baker, A. R., Jickells, T., Sarin, M., Bikkina, S., Gao, Y., Shelley, R. U., Buck, C. S., Landing, W. M., Bowie, A. R., Perron, M. M. G., Guieu, C., Meskhidze, N., Johnson, M. S., Feng, Y., Kok, J. F., Nenes, A., and Duce, R. A.: Pyrogenic iron: The missing link to high iron solubility in aerosols, *Sci. Adv.*, 5, eaau7671, <https://doi.org/10.1126/sciadv.aau7671>, 2019.
- Ito, T. and Follows, M. J.: Preformed phosphate, soft tissue pump and atmospheric CO₂, *J. Mar. Res.*, 63, 813–839, 2005.
- Jaccard, S. L. and Galbraith, E. D.: Large climate-driven changes of oceanic oxygen concentrations during the last deglaciation, *Nat. Geosci.*, 5, 151–156, <https://doi.org/10.1038/ngeo1352>, 2012.
- Jaccard, S. L., Hayes, C. T., Hodell, D. A., Anderson, R. F., Sigman, D. M., and Haug, G. H.: Two modes of change in Southern Ocean productivity over the past million years, *Science*, 339, 1419–1423, 2013.
- Jaccard, S. L., Galbraith, E. D., Martínez-García, A., and Anderson, R. F.: Covariation of deep Southern Ocean oxygenation and atmospheric CO₂ through the last ice age, *Nature*, 530, 207–10, <https://doi.org/10.1038/nature16514>, 2016.
- Khatriwala, S., Schmittner, A., and Muglia, J.: Air-sea disequilibrium enhances ocean carbon storage during glacial periods, *Sci. Adv.*, accepted, 2019.
- Key, R. M., Kozyr, A., Sabine, C. L., Lee, K., Wanninkhof, R., Bullister, J. L., Feely, R. A., Millero, F. J., Mordy, C., and Peng, T.-H.: A global ocean carbon climatology: Results from Global Data Analysis Project (GLODAP), *Global Biogeochem. Cy.*, 18, GB4031, <https://doi.org/10.1029/2004GB002247>, 2004.
- Kobayashi, H. and Oka, A.: Response of atmospheric pCO₂ to glacial changes in the Southern Ocean amplified by carbonate compensation, *Paleoceanography*, 33, 1206–1229, 2018.
- Kobayashi, H., Abe-Ouchi, A., and Oka, A.: Role of Southern Ocean stratification in glacial atmospheric CO₂ reduction evaluated by a three-dimensional ocean general circulation model, *Paleoceanography*, 30, 1202–1216, 2015.
- Kohfeld, K. E., Le Quére, C., Harrison, S. P., and Anderson, R. F.: Role of marine biology in glacial–interglacial CO₂ cycles, *Science*, 308, 74–78, <https://doi.org/10.1126/science.1105375>, 2005.
- Kohfeld, K. E., Graham, R. M., De Boer, A. M., Sime, L. C., Wolff, E. W., Le Quere, C., and Bopp, L.: Southern Hemisphere westerly wind changes during the Last Glacial Maximum: paleo-data synthesis, *Quaternary Sci. Rev.*, 68, 76–95, <https://doi.org/10.1016/j.quascirev.2013.01.017>, 2013.
- Lambert, F., Tagliabue, A., Shaffer, G., Lamy, F., Winckler, G., Farias, L., Gallardo, L., and De Pol-Holz, R.: Dust fluxes and iron fertilization in Holocene and Last Glacial Maximum climates, *Geophys. Res. Lett.*, 42, 6014–6023, <https://doi.org/10.1002/2015gl064250>, 2015.
- Lu, Z., Hoogakker, B. A. A., Hillenbrand, C.-D., Zhou, X., Thomas, E., Gutchess, K. M., Lu, W., Jones, L., and Rickaby, R. E. M.: Oxygen depletion recorded in upper waters of the glacial Southern Ocean, *Nat. Commun.*, 7, 11146, <https://doi.org/10.1038/ncomms11146>, 2016.
- Mahowald, N. M., Muhs, D. R., Levis, S., Rasch, P. J., Yoshioka, M., Zender, C. S., and Luo, C.: Change in atmospheric mineral aerosols in response to climate: last glacial period, preindustrial, modern, and doubled carbon dioxide climates, *J. Geophys. Res.*, 111, D10202, <https://doi.org/10.1029/2005JD006653>, 2006.
- Marinov, I., Gnanadesikan, A., Sarmiento, J. L., Toggweiler, J. R., Follows, M., and Mignone, B. K.: Impact of oceanic circulation on biological carbon storage in the ocean and atmospheric pCO₂, *Global Biogeochem. Cy.*, 22, GB3007, <https://doi.org/10.1029/2007GB002958>, 2008.
- Martin, J. H.: Glacial–interglacial CO₂ change: the iron hypothesis, *Paleoceanography*, 5, 1–13, 1990.
- Matsumoto, K.: Biology-mediated temperature control on atmospheric pCO₂ and ocean biogeochemistry, *Geophys. Res. Lett.*, 34, L20605, <https://doi.org/10.1029/2007GL031301>, 2007.
- Menviel, L., Joos, F., and Ritz, S. P.: Simulating atmospheric CO₂, ¹³C and the marine carbon cycle during the Last Glacial–Interglacial cycle: possible role for a deepening of the mean remineralization depth and an increase in the oceanic nutrient inventory, *Quaternary Sci. Rev.*, 56, 46–68, <https://doi.org/10.1016/j.quascirev.2012.09.012>, 2012.
- Menviel, L., Yu, J., Joos, F., Mouchet, A., Meissner, K., and England, M.: Poorly ventilated deep ocean at the Last Glacial Max-

- imum inferred from carbon isotopes: A data-model comparison study, *Paleoceanography*, 32, 2–17, 2017.
- Middleton, J. L., Langmuir, C. H., Mukhopadhyay, S., McManus, J. F., and Mitrovica, J. X.: Hydrothermal iron flux variability following rapid sea level changes, *Geophys. Res. Lett.*, 43, 3848–3856, <https://doi.org/10.1002/2016GL068408>, 2016.
- Moore, C. M., Mills, M. M., Arrigo, K. R., Berman-Frank, I., Bopp, L., Boyd, P. W., Galbraith, E. D., Geider, R. J., Guieu, C., Jaccard, S. L., Jickells, T. D., La Roche, J., Lenton, T. M., Mahowald, N. M., Marañón, E., Marinov, I., Moore, J. K., Nakatsuka, T., Oschilles, A., Saito, M. A., Thingstad, T. F., Tsuda, A., and Ulloa, O.: Processes and patterns of oceanic nutrient limitation, *Nat. Geosci.*, 6, 701–710, <https://doi.org/10.1038/ngeo1765>, 2013.
- Moore, J. K. and Braucher, O.: Sedimentary and mineral dust sources of dissolved iron to the world ocean, *Biogeosciences*, 5, 631–656, <https://doi.org/10.5194/bg-5-631-2008>, 2008.
- Muglia, J., Somes, C., Nickelsen, L., and Schmittner, A.: Combined effects of atmospheric and seafloor iron fluxes to the glacial ocean, *Paleoceanography*, 32, 1204–1218, 2017.
- Muglia, J., Skinner, L. C., and Schmittner, A.: Weak overturning circulation and high Southern Ocean nutrient utilization maximized glacial ocean carbon, *Earth Planet Sc. Lett.*, 496, 47–56, <https://doi.org/10.1016/j.epsl.2018.05.038>, 2018.
- Obase, T., Abe-Ouchi, A., Kusahara, K., Hasumi, H., and Ohgaito, R.: Responses of basal melting of Antarctic ice shelves to the climatic forcing of the Last Glacial Maximum and CO₂ doubling, *J. Climate*, 30, 3473–3497, 2017.
- Ohgaito, R., Abe-Ouchi, A., O’ishi, R., Takemura, T., Ito, A., Hajima, T., Watanabe, S., and Kawamiya, M.: Effect of high dust amount on surface temperature during the Last Glacial Maximum: a modelling study using MIROC-ESM, *Clim. Past*, 14, 1565–1581, <https://doi.org/10.5194/cp-14-1565-2018>, 2018.
- Oka, A., Abe-Ouchi, A., Chikamoto, M. O., and Ide, T.: Mechanisms controlling export production at the LGM: Effects of changes in oceanic physical field and atmospheric dust deposition, *Global Biogeochem. Cy.*, 25, GB2009, <https://doi.org/10.1029/2009GB003628>, 2011.
- Parekh, P., Follows, M. J., and Boyle, E. A.: Decoupling of iron and phosphate in the global ocean, *Global Biogeochem. Cy.*, 19, GB2020, <https://doi.org/10.1029/2004GB002280>, 2005.
- Parekh, P., Follows, M. J., Dutkiewicz, S., and Ito, T.: Physical and biological regulation of the soft tissue carbon pump, *Paleoceanography*, 21, PA3001, <https://doi.org/10.1029/2005PA001258>, 2006.
- Parekh, P., Joos, F., and Muller, S. A.: A modeling assessment of the interplay between aeolian iron fluxes and iron-binding ligands in controlling carbon dioxide fluctuations during Antarctic warm events, *Paleoceanography*, 23, Pa4202, <https://doi.org/10.1029/2007pa001531>, 2008.
- Roth, R., Ritz, S. P., and Joos, F.: Burial-nutrient feedbacks amplify the sensitivity of atmospheric carbon dioxide to changes in organic matter remineralisation, *Earth Syst. Dynam.*, 5, 321–343, <https://doi.org/10.5194/esd-5-321-2014>, 2014.
- Russell, J. L. and Dickson, A. G.: Variability in oxygen and nutrients in South Pacific Antarctic Intermediate Water, *Global Biogeochem. Cy.*, 17, 1033, <https://doi.org/10.1029/2000gb001317>, 2003.
- Sarmiento, J. L. and Gruber, N.: *Ocean Biogeochemical Dynamics*, chap. 8, Carbon cycle, 318–358, Princeton Univ. Press, Princeton, NJ, 2006.
- Schmiedl, G. and Mackensen, A.: Multispecies stable isotopes of benthic foraminifers reveal past changes of organic matter decomposition and deepwater oxygenation in the Arabian Sea, *Paleoceanography*, 21, 1–14, <https://doi.org/10.1029/2006PA001284>, 2006.
- Schmittner, A. and Somes, C. J.: Complementary constraints from carbon (C-13) and nitrogen (N-15) isotopes on the glacial ocean’s soft-tissue biological pump, *Paleoceanography*, 31, 669–693, 2016.
- Schroth, A. W., Crusius, J., Sholkovitz, E. R., and Bostick, B. C.: Iron solubility driven by speciation in dust sources to the ocean, *Nat. Geosci.*, 2, 337–340, 2009.
- Shoenfelt, E. M., Winckler, G., Lamy, F., Anderson, R. F., and Bostick, B. C.: Highly bioavailable dust-borne iron delivered to the Southern Ocean during glacial periods, *P. Natl. Acad. Sci. USA*, 115, 11180–11185, 2018.
- Sigman, D. M., Hain, M. P., and Haug, G. H.: The polar ocean and glacial cycles in atmospheric CO₂ concentration, *Nature*, 466, 47–55, <https://doi.org/10.1038/nature09149>, 2010.
- Skinner, L. C., Fallon, S., Waelbroeck, C., Michel, E., and Barker, S.: Ventilation of the deep Southern Ocean and deglacial CO₂ rise, *Science*, 328, 1147–1151, 2010.
- Somes, C. J., Schmittner, A., Muglia, J., and Oschlies, A.: A Three-Dimensional Model of the Marine Nitrogen Cycle during the Last Glacial Maximum Constrained by Sedimentary Isotopes, *Front. Mar. Sci.*, 4, 108, <https://doi.org/10.3389/fmars.2017.00108>, 2017.
- Tagliabue, A., Bopp, L., Roche, D. M., Bouttes, N., Dutay, J.-C., Alkama, R., Kageyama, M., Michel, E., and Paillard, D.: Quantifying the roles of ocean circulation and biogeochemistry in governing ocean carbon-13 and atmospheric carbon dioxide at the last glacial maximum, *Clim. Past*, 5, 695–706, <https://doi.org/10.5194/cp-5-695-2009>, 2009.
- Tagliabue, A., Bopp, L., Dutay, J. C., Bowie, A. R., Chever, F., Jean-Baptiste, P., Bucciarelli, E., Lannuzel, D., Remenyi, T., Sarthou, G., Aumont, O., Gehlen, M., and Jeandel, C.: Hydrothermal contribution to the oceanic dissolved iron inventory, *Nat. Geosci.*, 3, 252–256, 2010.
- Tamburini, F. and Föllmi, K. B.: Phosphorus burial in the ocean over glacial-interglacial time scales, *Biogeosciences*, 6, 501–513, <https://doi.org/10.5194/bg-6-501-2009>, 2009.
- Tschumi, T., Joos, F., Gehlen, M., and Heinze, C.: Deep ocean ventilation, carbon isotopes, marine sedimentation and the deglacial CO₂ rise, *Clim. Past*, 7, 771–800, <https://doi.org/10.5194/cp-7-771-2011>, 2011.
- Umling, N. E. and Thunell, R. C.: Mid-depth respired carbon storage and oxygenation of the eastern equatorial Pacific over the last 25,000 years, *Quaternary Sci. Rev.*, 189, 43–56, 2018.
- Vaquier-Sunyer, R. and Duarte, C. M.: Thresholds of hypoxia for marine biodiversity, *P. Natl. Acad. Sci. USA*, 105, 15452–15457, 2008.
- Völker, C. and Tagliabue, A.: Modeling organic iron-binding ligands in a three-dimensional biogeochemical ocean model, *Mar. Chem.*, 173, 67–77, <https://doi.org/10.1016/j.marchem.2014.11.008>, 2015.

- Wallmann, K., Schneider, B., and Sarnthein, M.: Effects of eustatic sea-level change, ocean dynamics, and nutrient utilization on atmospheric $p\text{CO}_2$ and seawater composition over the last 130 000 years: a model study, *Clim. Past*, 12, 339–375, <https://doi.org/10.5194/cp-12-339-2016>, 2016.
- Yamamoto, A., Abe-Ouchi, A., Shigemitsu, M., Oka, A., Takahashi, K., Ohgaito, R., and Yamanaka, Y.: Global deep ocean oxygenation by enhanced ventilation in the Southern Ocean under longterm global warming, *Global Biogeochem. Cy.*, 29, 1801–1815, 2015.
- Yamamoto, A., Abe-Ouchi, A., and Yamanaka, Y.: Long-term response of oceanic carbon uptake to global warming via physical and biological pumps, *Biogeosciences*, 15, 4163–4180, <https://doi.org/10.5194/bg-15-4163-2018>, 2018.